Acylated and unacylated ghrelin impair skeletal muscle atrophy in mice

Paolo E. Porporato,[1] Nicoletta Filigheddu,[1] Simone Reano,[1] Michele Ferrara,[1] Elia Angelino,[1] Viola F. Gnocchi,[1] Flavia Prodam,[2] Giulia Ronchi,[3] Sharmila Fagoonee,[4] Michele Fornaro,[3] Federica Chianale,[1] Gianluca Baldanzi,[1] Nicola Surico,[1] Fabiola Sinigaglia,[1] Isabelle Perroteau,[5] Roy G. Smith,[6] Yuxiang Sun,[7] Stefano Geuna,[3] and Andrea Graziani[1]

[1]Department of Translational Medicine, Interdisciplinary Research Center of Autoimmune Diseases (IRCAD), and Biotechnology Center for Applied Medical Research (BRMA), Università del Piemonte Orientale "Amedeo Avogadro" — Alessandria, Novara, Vercelli, Italy. [2]Department of Health Sciences, Università del Piemonte Orientale "Amedeo Avogadro" — Alessandria, Novara, Vercelli, Italy. [3]Neuroscience Institute "Cavalieri Ottolenghi" (NICO) and Department of Clinical and Biological Sciences, University of Torino, Orbassano (TO), Italy. [4]Molecular Biotechnology Center and Department of Genetics, Biology and Biochemistry, and [5]Department of Life Sciences and Systems Biology, University of Torino, Torino, Italy. [6]Department of Metabolism and Aging, The Scripps Research Institute, Scripps, Florida, USA. [7]USDA ARS Children's Nutrition Research Center, Departments of Pediatrics and Molecular and Cellular Biology, Baylor College of Medicine, Houston, Texas, USA.

Cachexia is a wasting syndrome associated with cancer, AIDS, multiple sclerosis, and several other disease states. It is characterized by weight loss, fatigue, loss of appetite, and skeletal muscle atrophy and is associated with poor patient prognosis, making it an important treatment target. Ghrelin is a peptide hormone that stimulates growth hormone (GH) release and positive energy balance through binding to the receptor GHSR-1a. Only acylated ghrelin (AG), but not the unacylated form (UnAG), can bind GHSR-1a; however, UnAG and AG share several GHSR-1a–independent biological activities. Here we investigated whether UnAG and AG could protect against skeletal muscle atrophy in a GHSR-1a–independent manner. We found that both AG and UnAG inhibited dexamethasone-induced skeletal muscle atrophy and atrogene expression through PI3Kβ-, mTORC2-, and p38-mediated pathways in myotubes. Upregulation of circulating UnAG in mice impaired skeletal muscle atrophy induced by either fasting or denervation without stimulating muscle hypertrophy and GHSR-1a–mediated activation of the GH/IGF-1 axis. In *Ghsr*-deficient mice, both AG and UnAG induced phosphorylation of Akt in skeletal muscle and impaired fasting-induced atrophy. These results demonstrate that AG and UnAG act on a common, unidentified receptor to block skeletal muscle atrophy in a GH-independent manner.

Introduction

Skeletal muscle atrophy involves massive loss of muscle structural proteins, which leads to muscle weight decrease and progressive loss of muscle function. Skeletal muscle atrophy is induced by muscle denervation and disuse, and it is also the key component of cachexia, a catabolic, debilitating response to several diseases. Cachectic patients not only sustain a decreased quality of life, but also face a worse prognosis of the underlying pathology, making cachexia an important target for treatment (1). Ghrelin is a circulating peptide hormone, octanoylated on Ser3, that is mainly produced by the stomach, which, by acting on the hypothalamus and the pituitary, induces GH secretion and stimulates food intake and adiposity through binding to its receptor, GHSR-1a (2–5). In addition to its endocrine activities, ghrelin protects cardiac function after heart damage (6, 7). In vitro, ghrelin inhibits the apoptosis of cardiomyocytes and other cell types by activating PI3K/Akt and ERK-1/2 pathways (8–10). Acylated ghrelin (AG) and unacylated ghrelin (UnAG) are generated from the same precursor, which can be acylated by the specific intracellular ghrelin-O-acyltransferase GOAT (11, 12). UnAG, which is far more abundant in plasma than AG, does not bind to GHSR-1a, lacks any GH-releasing activity (13), and has been considered for many years to be the inactive product of ghrelin catabolism. However, UnAG shares with AG common high-affinity binding sites on several cell types lacking GHSR-1a, including myocardial and skeletal myocytes, where they stimulate survival and differentiation, respectively (8, 9, 14–16). Furthermore, UnAG regulates gene expression in fat, muscle, and liver independently of GHSR-1a (17).

In both human patients and experimental models, AG ameliorates cachexia induced by several pathological conditions (6, 7, 13, 18–21). Although AG may inhibit cachexia by stimulating food intake, positive energy balance, and release of GH and IGF-1, the mechanisms underlying its anticachectic activity have not been fully elucidated.

Since we have previously shown that AG and UnAG, independently of GHSR-1a, inhibit apoptosis of cardiomyocytes by activating PI3K/Akt (8), a major antiatrophic signaling pathway (22, 23), and stimulate C2C12 skeletal myoblast differentiation (16), we investigated whether AG and UnAG could protect skeletal muscle from atrophy. Here, we provided evidence in vitro and in vivo that AG and UnAG, independently of GHSR-1a and activation of the GH/IGF-1 axis, trigger an antiatrophic signaling pathway by acting directly on the skeletal muscle, thereby protecting it from experimentally induced atrophy.

Results

AG and UnAG prevent dexamethasone-induced atrophy in C2C12-derived myotubes via mTORC2. C2C12 myotubes are a widely used model to study in vitro skeletal muscle atrophy induced by the synthetic glucocorticoid dexamethasone (24–26). Muscle atrophy was measured

Authorship note: Paolo E. Porporato and Nicoletta Filigheddu contributed equally to this work.

Conflict of interest: The authors have declared that no conflict of interest exists.

Citation for this article: *J Clin Invest.* doi:10.1172/JCI39920.

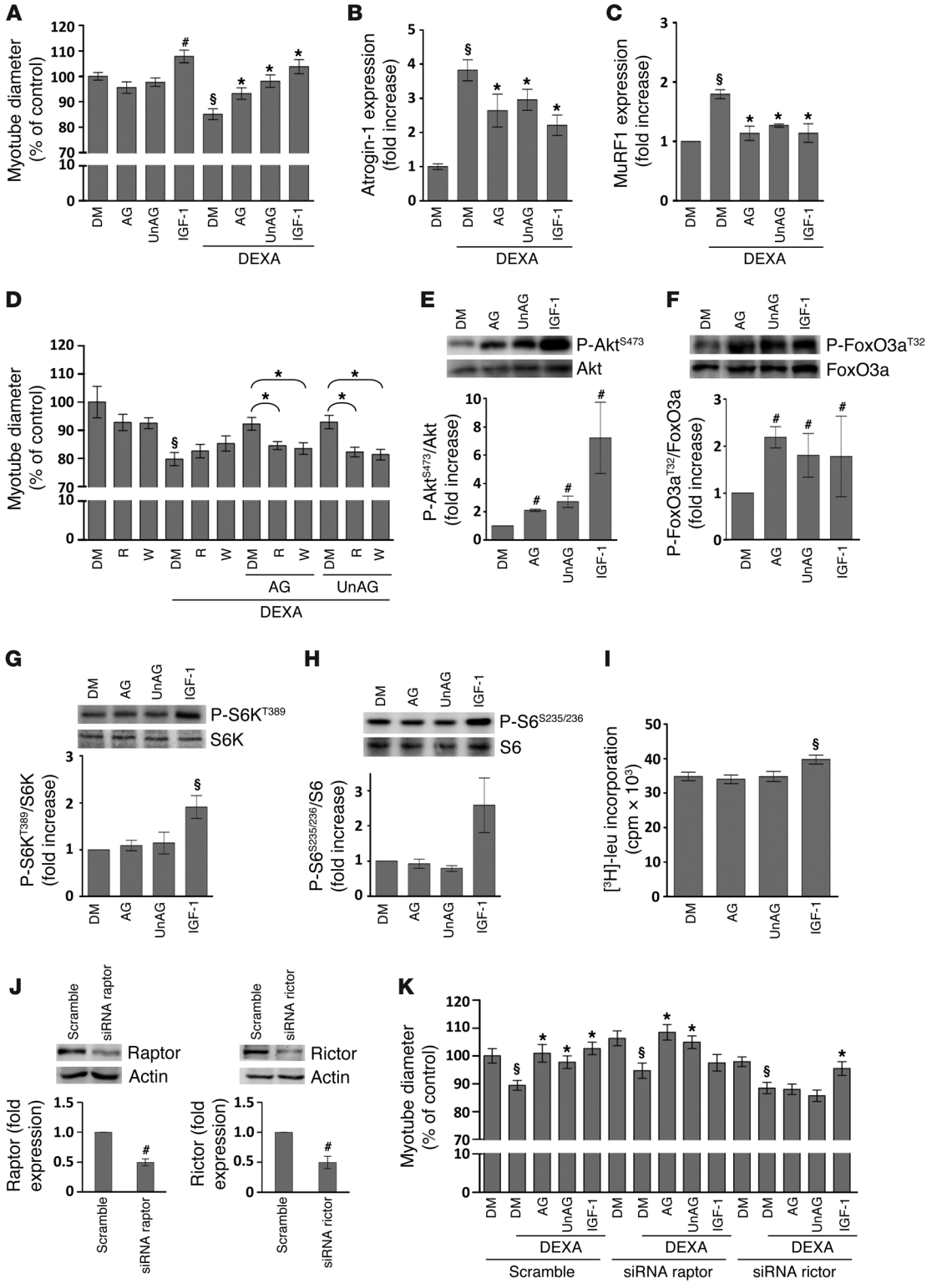
A
Myotube diameter (% of control)
DM
AG
UnAG
IGF-1
DEXA
B
Atrogin-1 expression (fold increase)
C
MuRF1 expression (fold increase)
D
Myotube diameter (% of control)
R
W
E
P-Akt^{S473}
Akt
P-Akt^{S473}/Akt (fold increase)
F
P-FoxO3a^{T32}
FoxO3a
P-FoxO3a^{T32}/FoxO3a (fold increase)
G
P-S6K^{T389}
S6K
P-S6K^{T389}/S6K (fold increase)
H
P-S6$^{S235/236}$
S6
P-S6$^{S235/236}$/S6 (fold increase)
I
[^{3}H]-leu incorporation (cpm x 10^3)
J
Scramble
siRNA raptor
Raptor
Actin
Raptor (fold expression)
siRNA rictor
Rictor
Rictor (fold expression)
K
Myotube diameter (% of control)
Scramble
siRNA raptor
siRNA rictor

Figure 1
AG and UnAG protect C2C12 myotubes from dexamethasone-induced atrophy without induction of protein synthesis or hypertrophy. (**A**) Myotube diameters were measured after 24-hour treatment in differentiation medium (DM) with 10 nM AG, 10 nM UnAG, and/or 1 μM dexamethasone (DEXA). In every experiment, 10 ng/ml IGF-1 was used as positive control for antiatrophic/hypertrophic activity. (**B** and **C**) Atrogin-1 and MuRF1 expression analysis upon dexamethasone treatment with or without AG and UnAG. (**D**) Treatment with 100 nM wortmannin (W) or 20 ng/ml rapamycin (R) reverted the antiatrophic activity of AG and UnAG on myotube diameter. Control myotubes in differentiation medium were treated with DMSO, a vehicle for both wortmannin and rapamycin. (**E** and **F**) Phosphorylation of Akt^{S473} and $FoxO3a^{T32}$, detected by Western blotting, upon treatment for 20 minutes with 1 μM AG or UnAG. Shown are representative blots and quantification of 3 independent experiments. (**G–I**) IGF-1, but not AG and UnAG, induced protein synthesis, as determined by phosphorylation of $S6K^{T389}$ (**G**) or $S6^{S235/236}$ (**H**) and by incorporation of [^{3}H]-leucine (**I**). (**J**) Effect of raptor and rictor silencing on protein levels, detected by Western blotting. (**K**) Silencing of rictor, but not of raptor, reverted the antiatrophic activity of AG and UnAG on the diameter of myotubes treated as in **A**. $^{\#}P < 0.05$, $^{\S}P < 0.01$ vs. DM control; $^{*}P < 0.01$ vs. DEXA treatment.

both as reduction of myotube diameter and as expression of the muscle-specific ubiquitin ligases Atrogin-1 (also known as MAFbx) and MuRF1, which drive muscle protein degradation in several models of muscle atrophy (24–27). Myotubes were treated with 1 μM dexamethasone for 24 hours in the presence or absence of 10 nM AG or UnAG, or with 10 ng/ml IGF-1 as a positive control of atrophy protection. Treatment with dexamethasone reduced myotube diameters by 20% and induced Atrogin-1 and MuRF1 expression. AG and UnAG impaired both these effects (Figure 1, A–C).

Skeletal muscle atrophy and atrogene expression can be opposed by the activation of mammalian target of rapamycin (mTOR), which, by forming 2 distinct protein complexes, mTORC1 and mTORC2, triggers distinct pathways that lead, respectively, to increased protein synthesis and to inhibited protein degradation (28, 29). To assess whether mTOR mediates the signaling triggered by AG/UnAG, myotubes were incubated with rapamycin, an inhibitor of mTORC1, which, upon prolonged treatment, also impairs the assembly of mTORC2 in several cell types, including C2C12 cells (refs. 30–32 and Supplemental Figure 1, A and B; supplemental material available online with this article; doi:10.1172/JCI39920DS1).

Upon 24-hour treatment of atrophying myotubes with 20 ng/ml rapamycin, the antiatrophic activity of AG/UnAG on myotube diameter was fully reverted (Figure 1D), which indicates that activation of mTOR is indeed required for the antiatrophic activity of AG and UnAG. Moreover, in the same assay, the antiatrophic activity of AG/UnAG was inhibited by 100 nM wortmannin, an inhibitor of PI3K, whose product $PI(3,4,5)P_3$ is essential for the activity of Akt, a substrate of mTORC2 that also mediates the activation of mTORC1 (29). These findings indicate that AG/UnAG antiatrophic activity requires both mTOR and Akt. Thus, we assayed the activity of both mTOR complexes. We evaluated mTORC2 activity as phosphorylation of Akt^{S473}, which, in turn, phosphorylates $FoxO3a^{T32}$, thus preventing Atrogin-1 transcription (24, 25). AG/UnAG, as well as IGF-1, induced phosphorylation of Akt^{S473} and $FoxO3a^{T32}$ (Figure 1, E and F), which indicates that they activate mTORC2-mediated pathways.

The activity of mTORC1 was assayed as phosphorylation of $S6K^{T389}$, a direct substrate of mTORC1, and of its substrate $S6^{S235/236}$, a ribosomal protein whose phosphorylation mediates protein synthesis (29). AG and UnAG did not induce phosphorylation of $S6K^{T389}$ and $S6^{S235/236}$ (Figure 1, G and H), nor protein synthesis (as measured by [^{3}H]-leucine incorporation; Figure 1I) or myotube hypertrophy (Figure 1A). Conversely, IGF-1 induced $S6K^{T389}$ and $S6^{S235/236}$ phosphorylation, [^{3}H]-leucine incorporation, and myotube diameter increase, as expected.

By silencing raptor and rictor, specific components of mTORC1 and mTORC2, respectively (Figure 1J), we observed that downregulation of rictor abrogated the protective effect of both peptides on dexamethasone-induced muscle atrophy, measured as myotube diameter, while it did not affect the antiatrophic activity of IGF-1 (Figure 1K). Conversely, raptor silencing impaired IGF-1 antiatrophic activity without affecting that of AG/UnAG. These results indicate that mTORC2 pathway mediates AG/UnAG antiatrophic activity in C2C12 myotubes, without involving mTORC1-mediated protein synthesis.

To identify the signaling pathways differently activated by AG/UnAG and IGF-1, we investigated the role of p38 serine kinase, whose activation by AG/UnAG mediates C2C12 myoblast differentiation (16). In C2C12 myotubes, AG/UnAG, as well as IGF-1, induced phosphorylation of $p38^{T180/Y182}$ (Figure 2A), and its pharmacological inhibition impaired the antiatrophic activity of AG/UnAG, but not of IGF-1 (Figure 2B).

Activation of p38 has been reported to downregulate Atrogin-1, thereby contributing to the protection of skeletal muscle from atrophy (33). On the other hand, p38 mediates induction of Atrogin-1 by TNF-α and oxidative stress and of MuRF1 by serum starvation (34–37). Inhibition of p38 with SB203580 reduced dexamethasone-induced expression of both Atrogin-1 and MuRF1; nevertheless, induction of Atrogin-1, but not MuRF1, was still significant (Figure 2, C and D). In the presence of SB203580, AG and UnAG, but not IGF-1, failed to further reduce the residual induction of Atrogin-1, which indicates that p38 mediates AG/UnAG signaling in regulating Atrogin-1 expression.

To further characterize AG/UnAG antiatrophic activity, we treated C2C12 myotubes with NF449, a compound uncoupling $G\alpha_s$ from GPCRs, which inhibits antiapoptotic activity of AG and UnAG in pancreatic β cells (9, 38). NF449 completely abrogated Akt^{S473} phosphorylation and antiatrophic activity of AG/UnAG without affecting IGF-1 activities (Figure 2, E and F), which supports the hypothesis that AG and UnAG act through a GPCR, as previously suggested (9).

PI3K α and β isoforms mediate Akt activation upon stimulation of tyrosine kinase receptors and GPCRs, respectively (39, 40). We dissected the contribution of PI3Kα and PI3Kβ to IGF-1 and AG/UnAG antiatrophic activity using isoform-specific PI3K inhibitors. Whereas inhibition of PI3Kα by PIK-75 abolished IGF-1 antiatrophic activity, it did not affect AG/UnAG protection. Conversely, inhibition of PI3Kβ by TGX-221 impaired AG/UnAG antiatrophic activity while not affecting IGF-1 protection (Figure 2G). The involvement of PI3Kβ in AG/UnAG antiatrophic activity was further supported by the finding that TGX-221 prevented AG/UnAG from reducing dexamethasone-induced Atrogin-1 expression (Figure 2H). Together, these data strongly suggest that AG/UnAG acts through GPCR-dependent signaling pathways involving a PI3K isoform distinct from that of IGF-1.

Glucocorticoids induce muscle mass reduction by also upregulating the expression of myostatin, a TGF-β family member that acts as a negative regulator of muscle mass. Myostatin reduces the

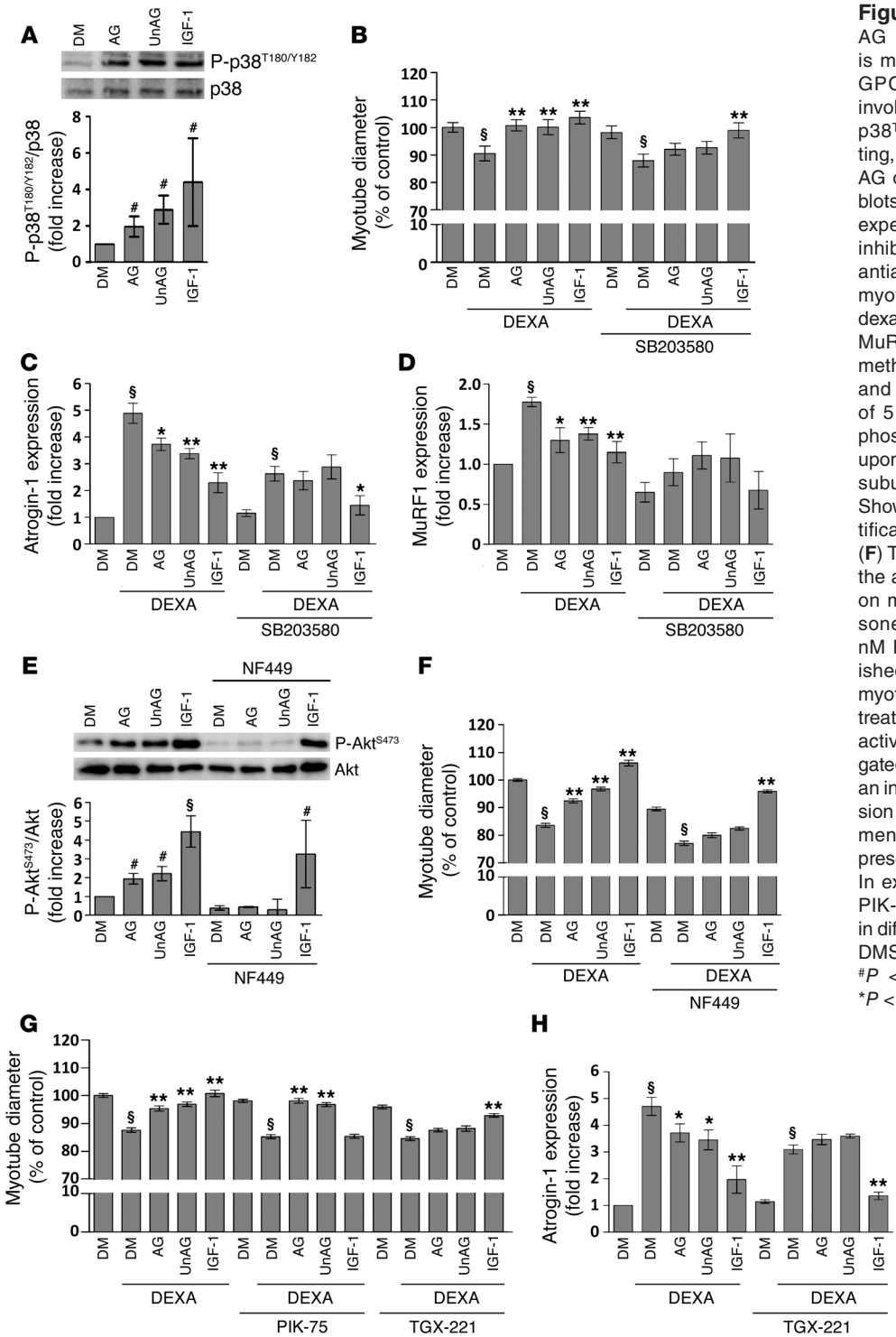

Figure 2

AG and UnAG antiatrophic signaling is mediated by p38 and acts through a GPCR-dependent signaling pathway involving PI3Kβ. (**A**) Phosphorylation of $p38^{T180/Y182}$, detected by Western blotting, after 20-minute treatment with 1 μM AG or UnAG. Shown are representative blots and quantification of 3 independent experiments. (**B**) Treatment with the p38 inhibitor SB203580 (5 μM) reverted the antiatrophic activity of AG and UnAG on myotube diameter upon treatment with dexamethasone. (**C** and **D**) Atrogin-1 and MuRF1 expression analysis upon dexamethasone treatment with or without AG and UnAG in the presence or absence of 5 μM SB203580. (**E**) AG and UnAG phosphorylation of Akt^{S473} was abolished upon treatment with 10 μM NF449, a $G\alpha_s$ subunit–selective G protein antagonist. Shown are representative blots and quantification of 3 independent experiments. (**F**) Treatment with 10 μM NF449 reverted the antiatrophic activity of AG and UnAG on myotube diameter upon dexamethasone treatment. (**G**) Treatment with 25 nM PIK-75, an inhibitor of PI3Kα, abolished the antiatrophic effect of IGF-1 on myotube diameter upon dexamethasone treatment, without affecting AG and UnAG activity. The antiatrophic effect was abrogated by treatment with 200 nM TGX-221, an inhibitor of PI3Kβ. (**H**) Atrogin-1 expression analysis upon dexamethasone treatment with AG, UnAG, and IGF-1 in the presence or absence of 200 nM TGX-221. In experiments with SB203580, NF449, PIK-75, and TGX-221, control myotubes in differentiation medium were treated with DMSO, a vehicle for all these compounds. $^{\#}P < 0.05$, $^{\S}P < 0.01$ vs. DM control; $^{*}P < 0.05$, $^{**}P < 0.01$ vs. DEXA treatment.

size of human skeletal muscle cell–derived myotubes by reducing mTOR/Akt/p70S6K signaling, while simultaneous treatment with IGF-1 restores myotube size, Akt phosphorylation, and protein synthesis (41, 42). In C2C12 myotubes, dexamethasone treatment actually induced the expression of myostatin, which was significantly reduced by IGF-1. However, AG/UnAG had no effect on myostatin expression (Supplemental Figure 1C), providing further evidence that ghrelin and IGF-1 inhibit muscle atrophy through distinct, partially overlapping, mechanisms.

Tg mice with high levels of circulating UnAG are protected from fasting- and denervation-induced atrophy. To verify in vivo the relevance of the findings described above, we used a strain of Tg mice with cardiac-specific ghrelin gene (*Ghrl*) expression. In these mice (referred to herein as *Myh6/Ghrl*), *Ghrl* overexpression in the heart results in

Table 1
Phenotypical characterization of *Myh6/Ghrl* mice

	WT	*Myh6/Ghrl*
UnAG (pg/ml)	445.4 ± 155	25,000.5 ± 360[A]
AG, fed (pg/ml)	41.7 ± 1.6	39.3 ± 1.5
AG, fasted (pg/ml)	75.7 ± 8.8	68.2 ± 9.5
IGF-1, fed (ng/ml)	748.5 ± 56	765.5 ± 120
IGF-1, fasted (ng/ml)	398 ± 93	328 ± 37
Insulin (pg/ml)	571 ± 58	631 ± 129
Tibial length (mm)	19.65 ± 0.11	19.62 ± 0.22
Nasoanal length (mm)	91.59 ± 0.51	90.61 ± 0.95
BMI, fed (g/cm^2)	3.32 ± 0.12	3.33 ± 0.08
BMI, fasted (g/cm^2)	2.93 ± 0.06	2.92 ± 0.09
Gastrocnemius weight, fed (mg)	134.86 ± 4.6	137.2 ± 5.62
Gastrocnemius weight, fasted (mg)	118 ± 4	124 ± 3.1
Gastrocnemius weight/tibial length, fed (mg/mm)	6.86 ± 0.22	6.99 ± 0.25
Gastrocnemius weight/tibial length, fasted (mg/mm)	5.89 ± 0.14	6.36 ± 0.15[B]
Heart weight, fed (mg)	117.5 ± 11.8	122 ± 6.8
Heart weight, fasted (mg)	103.0 ± 7.1	105 ± 3.3
Heart weight/nasoanal length, fed (mg/mm)	1.22 ± 0.12	1.28 ± 0.08
Heart weight/nasoanal length, fasted (mg/mm)	1.16 ± 0.07	1.16 ± 0.03
Daily food intake (g)	4.66 ± 0.17	4.73 ± 0.07
Daily food intake, denervated (g)	4.60 ± 0.17	4.60 ± 0.18

Measurements were performed as described in Methods. Muscle mass and tibial length were calculated as the mean of right and left hindlimbs. $n = 7$ per group (fed); 4 per group (fasted 48 hours); 5 per group (denervated). Data are mean ± SEM. [A]$P < 0.01$ vs. WT. [B]$P < 0.05$ vs. WT.

a 50-fold increase of circulating UnAG, without affecting AG levels (Table 1), as previously observed in other *Ghrl*-overexpressing Tg mice (43–45). *Ghrl* mRNA overexpression was restricted to the myocardium of *Myh6/Ghrl* mice, without leakage in the skeletal muscle (Supplemental Figure 2A). Moreover, consistent with the inability of UnAG to activate GHSR-1a and to promote GH release and adiposity, *Myh6/Ghrl* mice did not feature any change in circulating IGF-1 concentration, tibial and nasoanal length, BMI, or food intake compared with their WT littermates. In addition, fasting decreased IGF-1 and increased ghrelin circulating concentrations to the same extent in WT and *Myh6/Ghrl* mice (Table 1). These data strongly indicate that the upregulation of circulating UnAG in *Myh6/Ghrl* mice does not activate GHSR-1a in the pituitary and hypothalamus, stimulate the GH/IGF-1 axis, or affect endogenous ghrelin regulation. Moreover, tissue expression of IGF-1, which in skeletal muscle may act locally in a paracrine/autocrine manner (46), was not altered in *Myh6/Ghrl* mice, either in fed or in fasted animals (Supplemental Figure 2B).

Although AG and UnAG differently regulate insulin release and sensitivity (47), basal insulin level, glucose uptake, and insulin sensitivity were not affected in *Myh6/Ghrl* mice (Table 1 and Supplemental Figure 2, C and D).

Notably, compared with WT animals, fed *Myh6/Ghrl* mice did not feature any difference in heart and gastrocnemius muscle weight (Table 1), fiber cross-sectional area (CSA) distribution, or hindlimb force (as measured by grasping test; Supplemental Figure 2, E and F), which indicates that high levels of circulating UnAG do not induce skeletal muscle hypertrophy in vivo, consistent with the inability of UnAG to induce hypertrophy in C2C12-derived myotubes.

To investigate whether UnAG might protect from muscle wasting, we induced skeletal muscle atrophy by food deprivation. After 48 hours of fasting, gastrocnemius weight was decreased by approximately 14% in WT mice, and by approximately 9% in *Myh6/Ghrl* mice, compared with fed animals (Figure 3A), which indicates that increased circulating UnAG results in 30% protection from fasting-induced loss in gastrocnemius mass. Accordingly, gastrocnemii CSA was reduced by 29% in WT mice and by 19% in *Myh6/Ghrl* mice compared with fed animals (Figure 3B), indicative of 34% protection. Similarly, extensor digitorum longus (EDL) muscle weight and mean fiber area of *Myh6/Ghrl* mice was reduced to a lesser extent than in WT animals (Figure 3, D and E). This protection was reflected by shift in CSA distributions of gastrocnemii and EDL — toward fibers with wider area — in *Myh6/Ghrl* compared with WT mice under fasting conditions (Figure 3, C and F).

After 48 hours of fasting, Atrogin-1 and MuRF1 expression in gastrocnemii of WT animals dramatically increased. In *Myh6/Ghrl* mice, the induction of Atrogin-1 was significantly reduced by one-third, while MuRF1 was only slightly, not significantly, decreased (Figure 3, G and H).

Plasma levels of glycerol and FFAs did not change in fasted *Myh6/Ghrl* and WT mice (Supplemental Figure 2, G and H), which indicates that fasting did not significantly affect either glycerol or FFA concentrations, consistent with previous reports in the FVB mouse background (48, 49). Moreover, hepatic phosphoenolpyruvate carboxykinase (PEPCK) expression was induced to the same extent in fasted *Myh6/Ghrl* and WT littermates (Supplemental Figure 2I). Together, these data suggest that muscle wasting–resistant properties of *Myh6/Ghrl* mice do not depend on effects of UnAG on energy balance.

Furthermore, *Myh6/Ghrl* mice were protected from denervation-induced muscle atrophy, an experimental procedure that does not affect animal daily food intake (Table 1). At 7 and 14 days after denervation, gastrocnemii weight of WT animals was reduced by 21% and 27%, respectively, while the loss of muscle weight in *Myh6/Ghrl* animals was significantly lower (Figure 4A). Consistently, gastrocnemii mean fiber CSA of WT animals was remarkably reduced at both 7 and 14 days after denervation, whereas CSA in *Myh6/Ghrl* animals was reduced to a lesser extent (Figure 4B). At 7 days after denervation, *Myh6/Ghrl* mice featured a mild shift of gastrocnemii CSA distribution that became impressive after 14 days (Figure 4, C and D). A strong inhibition of atrophy at 7 days after denervation was also evident in EDL (Figure 4, E and F) and tibialis anterior (TA) muscles (Figure 4, G and H).

Moreover, in gastrocnemii of *Myh6/Ghrl* mice, the induction of Atrogin-1 was reduced by 40% (Figure 4I). Conversely, MuRF1 was only slightly, not significantly, reduced (Figure 4J), consistent with the fasting-induced atrophy data. Together, these observations indicated that constitutive high levels of UnAG impair experimentally induced atrophy in vivo, likely through a mechanism independent of GHSR-1a and activation of the GH/IGF-1 axis.

UnAG pharmacological treatment induces antiatrophic signaling in muscle and inhibits fasting- and denervation-induced atrophy. Acute

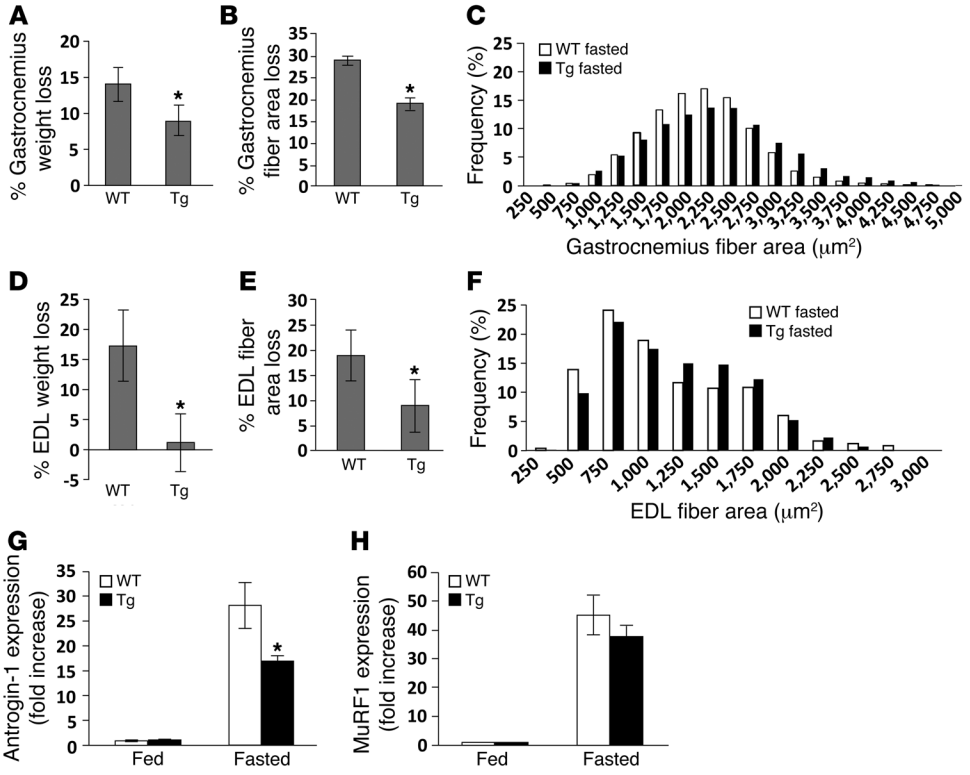

Figure 3

Myh6/Ghrl mice are protected from skeletal muscle atrophy induced by 48 hours of fasting. (**A**–**C**) Effect of fasting on gastrocnemii. Mean percentage of gastrocnemius weight loss (**A**) and CSA reduction (**B**) of fasted *Myh6/Ghrl* (Tg) mice and WT littermates compared with fed animals. (**C**) Frequency distribution of gastrocnemii CSA of fasted *Myh6/Ghrl* and WT mice. (**D**–**F**) Effect of fasting on EDL muscles. Mean percentage of EDL muscle weight loss (**D**), CSA reduction (**E**), and CSA frequency distribution (**F**) of fasted *Myh6/Ghrl* and WT littermates. (**G** and **H**) Atrogin-1 and MuRF1 expression in gastrocnemii of fed and fasted *Myh6/Ghrl* mice and their WT littermates, determined by real-time RT-PCR. **P* < 0.01 vs. WT. *n* = 7 (fed WT and *Myh6/Ghrl*); 5 (fasted WT); 6 (fasted *Myh6/Ghrl*); 3 (CSA loss and distribution, WT and *Myh6/Ghrl*).

administration of exogenous UnAG at 100 μg/kg, a dose previously used for in vivo studies (6), induced phosphorylation of Akt^{S473}, $FoxO3a^{T32}$, and $p38^{T180/Y182}$ in WT gastrocnemii (Figure 5, A–C), which indicates that, in vivo, UnAG activates the same antiatrophic signaling pathway as it does in C2C12 myotubes.

Repeated administration (every 12 hours) of UnAG protected mice from skeletal muscle atrophy induced by either fasting or denervation (Figure 5, D–I). UnAG treatment preserved gastrocnemii from weight and mean fiber CSA loss (Figure 5, D and E). Accordingly, frequency distribution of gastrocnemii CSA of fasted mice injected with UnAG showed a dramatic shift toward bigger fiber areas compared with saline-injected mice (Figure 5F).

Similarly, UnAG treatment of denervated mice resulted in a 25% protection from gastrocnemius weight loss and a significantly lower decrease of mean fiber CSA, although the CSA distribution of UnAG-injected mice showed only a very mild shift compared with saline-injected animals (Figure 5, G–I). Although the plasma concentration of UnAG after injection dropped to basal levels in about 2–4 hours (Supplemental Figure 3A), these data indicate that repeated acute stimulation is sufficient to protect from experimentally induced skeletal muscle atrophy without affecting muscular IGF-1 expression (Supplemental Figure 3B).

AG and UnAG induce antiatrophic signaling and impair muscle atrophy in Ghsr$^{-/-}$ *mice*. The findings reported above, along with previous data on common binding sites for AG/UnAG in C2C12 lacking *Ghsr* (16), strongly suggest that AG and UnAG stimulate antiatrophic signaling in skeletal muscle through activation of a receptor distinct from GHSR-1a. To verify this hypothesis, we assayed AG/UnAG antiatrophic signaling and activity in *Ghsr*$^{-/-}$ mice, in which AG fails to activate the GH/IGF-1a axis or stimulate appetite (50). Injection of either AG or UnAG induced Akt^{S473} phosphorylation in gastrocnemii of *Ghsr*$^{-/-}$ mice (Figure 6A). Consistently, treatment of *Ghsr*$^{-/-}$ mice with 100 μg/kg AG or UnAG twice daily reduced gastrocnemii weight loss induced by 48-hour fasting by 30% compared with saline-treated animals (Figure 6B). Moreover, the mean CSA loss of AG- and UnAG-injected mice strongly decreased compared with saline-injected animals, and CSA distribution shifted toward bigger areas (Figure 6, C and D).

In summary, these findings demonstrated that both AG and UnAG activate a direct antiatrophic signaling pathway in skeletal muscle and protect from experimentally induced muscle atrophy, independently of the AG receptor GHSR-1a.

Discussion

Several studies have shown that AG protects from cachexia and prevents muscle proteolysis in vivo, supposedly through stimulation of appetite and activation of the GH/IGF-1 axis mediated by AG binding to GHSR-1a (6, 7, 18–21). However, here we provided in vitro and in vivo evidence that AG and UnAG exert antiatrophic activity by acting directly on the skeletal muscle, even in *Ghsr*$^{-/-}$ mice.

Upregulation of circulating UnAG, which does not bind GHSR-1a and does not activate the GH/IGF-1 axis, counteracted muscle atrophy induced by either fasting or denervation. Consistently, UnAG has been reported to reduce burn-induced skeletal muscle proteolysis and local TNF-α upregulation (51).

We achieved upregulation of circulating UnAG either by myocardial *Ghrl* overexpression in *Myh6/Ghrl* mice or by repeated administration. The antiatrophic activity of UnAG cannot be mediated by its conversion to AG in the plasma, since acylation occurs only intracellularly on the ghrelin precursor by the ghrelin-specific acyltransferase GOAT (11, 12). The negligible myocardial expression of GOAT might explain the increase of only the unacylated form

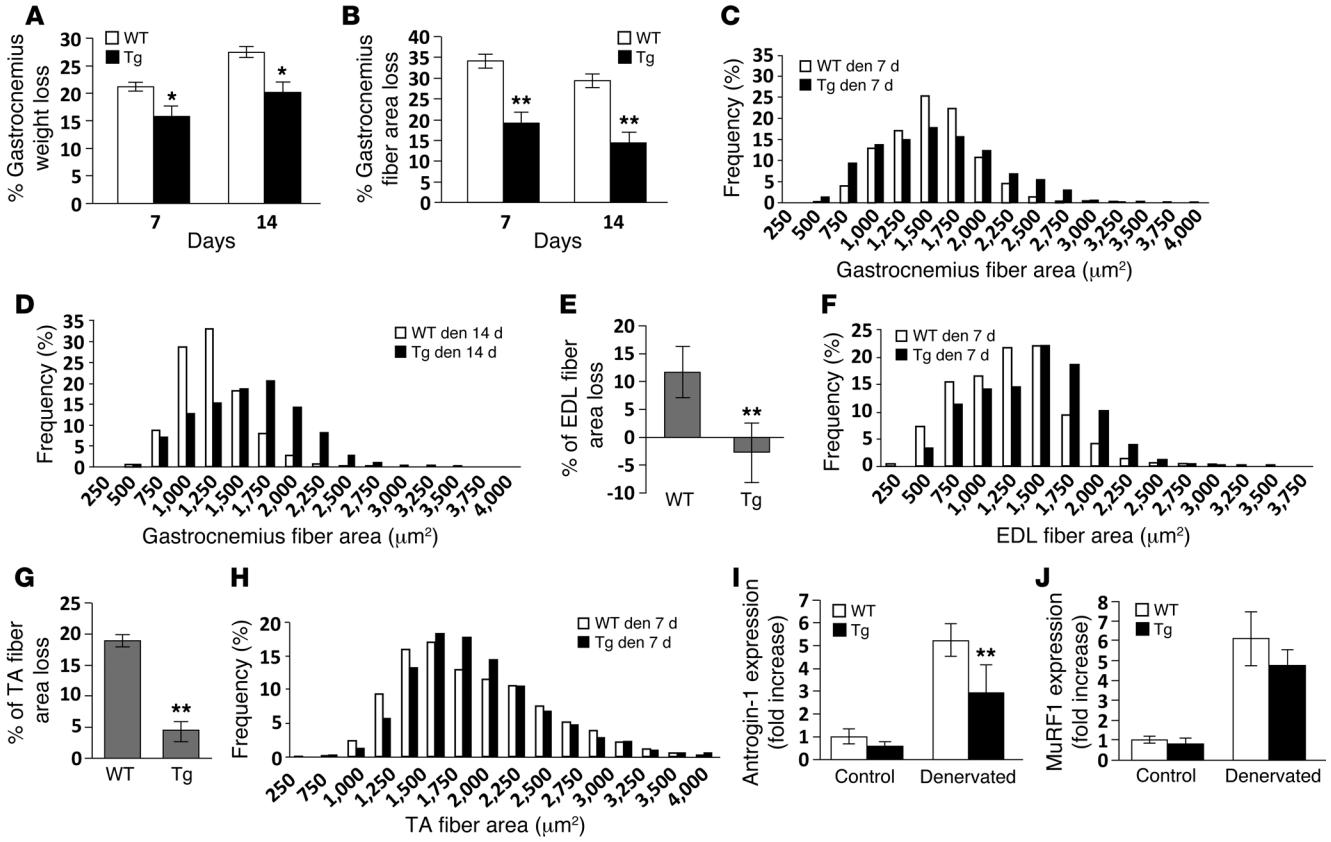

Figure 4

Myh6/Ghrl mice are protected from denervation-induced skeletal muscle atrophy induced by sciatic nerve resection. (**A** and **B**) Mean percentage of weight loss (**A**) and CSA reduction (**B**) of denervated gastrocnemius at 7 and 14 days after denervation, compared with the unperturbed side. (**C** and **D**) Frequency distribution of gastrocnemii CSA at 7 and 14 days after denervation in *Myh6/Ghrl* and WT mice. (**E**–**H**) CSA reduction and fiber area distribution of (**E** and **F**) EDL and (**G** and **H**) TA muscles at 7 days after denervation. (**I** and **J**) Atrogin-1 and MuRF1 expression, determined by real-time RT-PCR, in denervated gastrocnemii at 7 days after denervation, compared with the unperturbed side. $^{**}P < 0.01$, $^{*}P < 0.05$ vs. WT. $n = 6$ (WT); 5 (*Myh6/Ghrl*); 3 (CSA loss and distribution, WT and *Myh6/Ghrl*).

of circulating ghrelin in *Myh6/Ghrl* mice. This is in agreement with other tissue-specific *Ghrl* Tg mice featuring high UnAG circulating levels in the absence of significant changes of AG (43–45).

The observations that *Myh6/Ghrl* mice did not feature any change in circulating and muscular IGF-1 or in tibial or whole body length, along with the lack of skeletal muscle hypertrophy, further indicate that the GH/IGF-1 axis is not activated in these mice. Finally, the finding that both AG and UnAG impaired skeletal muscle atrophy in *Ghsr*$^{-/-}$ mice indicated that their antiatrophic activity is mediated by a receptor distinct from GHSR-1a. In these mice, AG exerted antiatrophic activity in the skeletal muscle independent of its role in modulating GH release and energy balance. Nevertheless, these data do not exclude the possibility that in WT animals, GHSR-1a may contribute to the antiatrophic activity of AG by also regulating the GH/IGF-1 axis and positive energy balance. For instance, AG has been suggested to prevent downregulation of muscular IGF-1 expression in an experimental model of cachexia through an indirect mechanism involving GHSR-1a activity on positive energy balance (20).

The hypothesis that AG/UnAG impairs muscle atrophy in vivo by acting directly on the skeletal muscle is further supported by our finding that UnAG administration rapidly stimulated antiatrophic signaling in the gastrocnemius. Moreover, AG/UnAG activated antiatrophic signaling in cultures of C2C12 myotubes, which do not express GHSR-1a, protecting them from dexamethasone-induced atrophy and atrogene upregulation. Although AG has previously been reported to fail in reducing dexamethasone-induced Atrogin-1 expression in C2C12 myotubes (20), the 10-fold lower dexamethasone concentration used in that study and the considerably weaker Atrogin-1 induction may explain the different results. Conversely, Sheriff et al. showed that UnAG reduces TNF-α/IFN-γ–induced cachexia in C2C12 myotubes in a PI3K/mTOR-dependent manner (51). The results of our present study not only confirmed the involvement of PI3K/mTOR pathways in AG/UnAG activity on skeletal muscle, but also showed the specific contribution of the mTORC2- over the mTORC1-mediated signaling pathway, which may explain, at least in part, the ability of AG/UnAG to protect from skeletal muscle atrophy without a concomitant induction of hypertrophy.

Indeed, the molecular mechanisms underlying AG/UnAG antiatrophic activity in the skeletal muscle involved the activation of mTORC2-mediated signaling pathways, leading to phosphorylation of Akt^{S473} and of its substrate FoxO3a^{T32}, which eventually impaired Atrogin-1 expression and muscle protein degradation. At

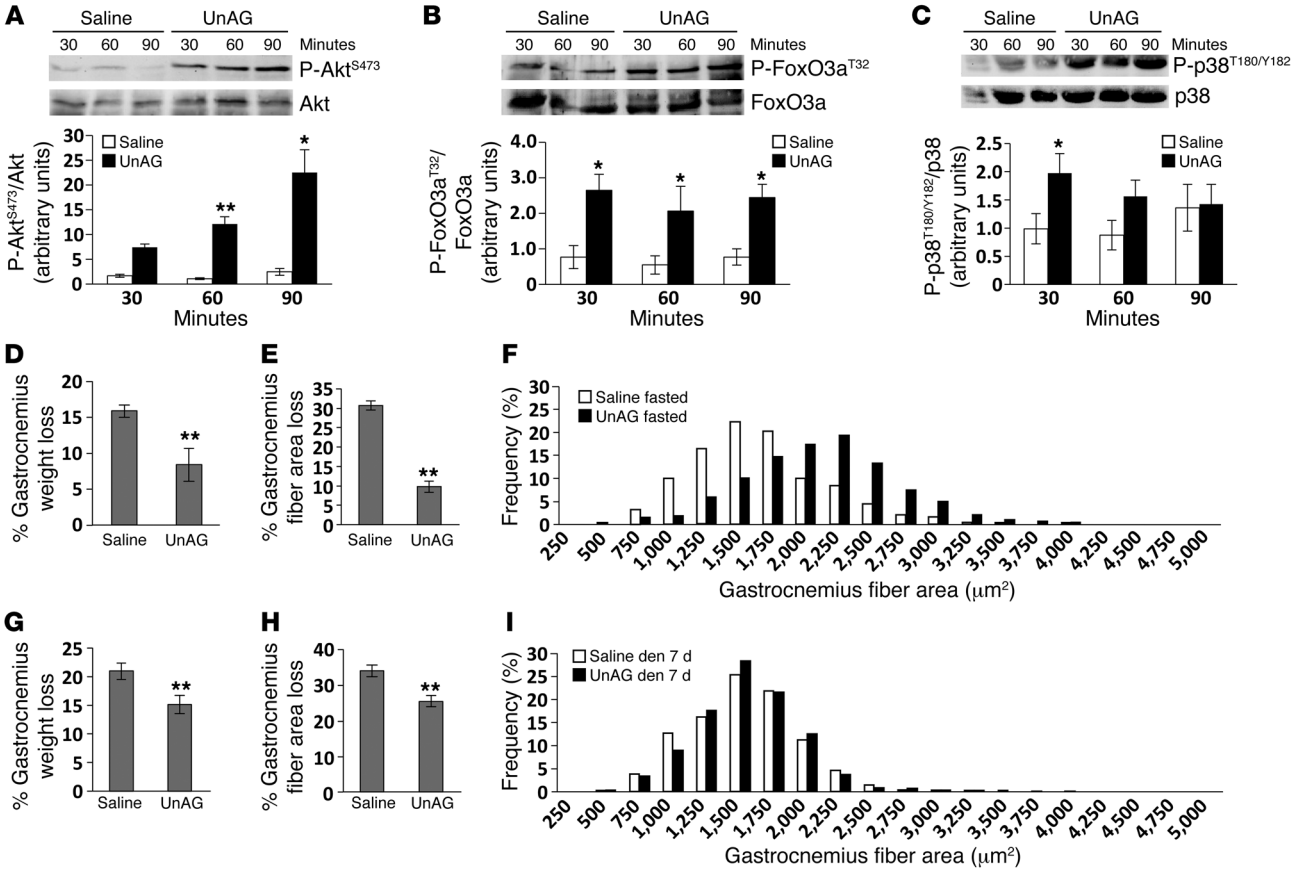

Figure 5

UnAG pharmacological treatment protects skeletal muscle from fasting- and denervation-induced atrophy in WT mice. (**A**–**C**) Phosphorylation of Akt^{S473}, FoxO3a^{T32}, and p38$^{T180/Y182}$ in gastrocnemii of WT mice treated with 100 μg/kg UnAG or saline. At the indicated time points, gastrocnemii were removed and processed for Western blot analysis. Shown are representative blots and densitometric analysis of 3 independent experiments, normalized to untreated animals (not shown). (**D**–**F**) Mean percent weight loss (**D**), CSA reduction (**E**), and CSA frequency distribution (**F**) of gastrocnemii from fed or 48-hour fasted mice treated twice daily with 100 μg/kg UnAG or saline (n = 5 per group). Frequency distribution was measured in 3 mice per group. In **D** and **E**, percent reduction shown is between fasted and fed mice. (**G**–**I**) Mean percent weight loss (**G**), CSA reduction (**H**), and CSA frequency distribution (**I**) of gastrocnemii from mice treated with 100 μg/kg UnAG or saline twice daily for 7 days after sciatic nerve resection (n = 5 per group). Frequency distribution was measured in 3 mice per group. In **G** and **H**, percent reduction shown is between denervated gastrocnemii and gastrocnemii from the unperturbed side. *P < 0.05, **P < 0.01 vs. saline treatment.

the same time, in C2C12 myotubes, AG/UnAG failed to stimulate mTORC1-mediated phosphorylation of S6K^{T389} and S6$^{S235/236}$, protein synthesis, and hypertrophy. Consistently, chronic upregulation of circulating UnAG in *Myh6/Ghrl* mice did not induce muscle hypertrophy. This finding highlights a remarkable difference between the antiatrophic activities of AG/UnAG and IGF-1 in the skeletal muscle, as IGF-1 stimulates both mTORC2-mediated impairment of protein degradation and mTORC1-dependent stimulation of protein synthesis and hypertrophy (23–26). Consistently, in TNF-α/IFN-γ–treated C2C12 myotubes, UnAG inhibited protein catabolism and impaired the induction of Atrogin-1 and MuRF1. Moreover, UnAG restored the basal phosphorylation state of proteins of mTORC1 and mTORC2 pathways, although the lack of UnAG-induced increase in Akt^{S473} phosphorylation observed herein may depend on receptor desensitization, given the higher concentration of UnAG used and the protracted treatment (51).

The finding that downregulation of the mTORC1-specific component raptor did not affect the antiatrophic activity of AG/UnAG, while impairing IGF-1 antiatrophic activity, further supports the conclusion that AG/UnAG antiatrophic activity does not involve mTORC1-mediated stimulation of protein synthesis. On the other hand, the finding that AG/UnAG antiatrophic activity was sensitive to downregulation of rictor, the specific component of mTORC2, demonstrated the key role of mTORC2 in mediating AG/UnAG antiatrophic activity. The finding that ghrelin-induced phosphorylation of Akt^{S473} was uncoupled from the activation of mTORC1-mediated pathways and hypertrophy may appear controversial, as IGF-1–induced phosphorylation of Akt^{S473} is associated with the activity of both mTOR complexes (29), and overexpression of constitutive active Akt in the skeletal muscle prevents denervation-induced atrophy and induces hypertrophy (22, 52). The lack of muscle hypertrophy observed in *Myh6/Ghrl* mice may depend on weaker stimulation of the PI3K/Akt pathway by UnAG. Indeed, although tissue-specific expression of constitutive active Akt in Tg mice induces strong phosphorylation of Akt and of its substrates (53), phosphorylation of Akt was not detectable in

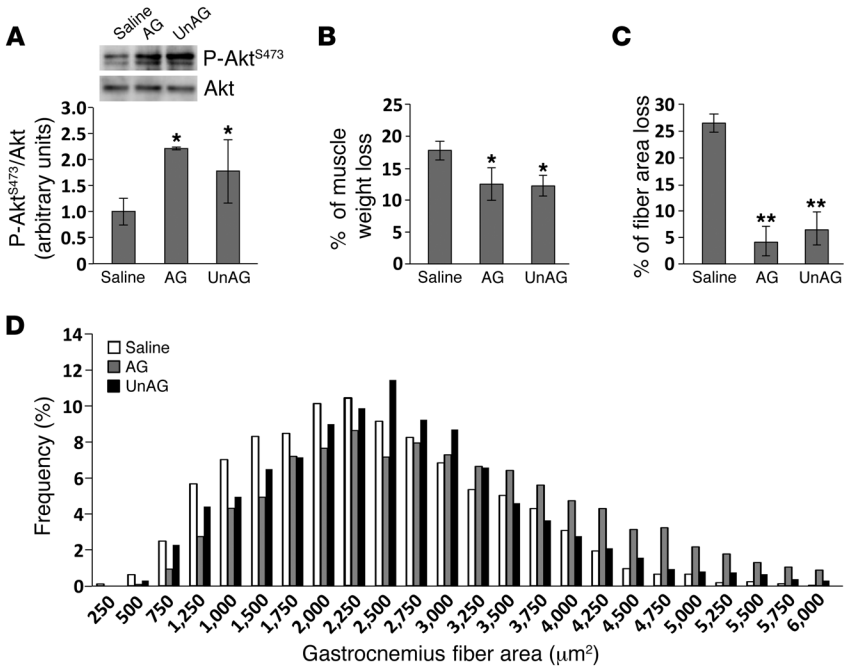

Figure 6
AG and UnAG pharmacological treatment of *Ghsr*$^{-/-}$ mice induces antiatrophic signaling and protects from fasting-induced skeletal muscle atrophy. (**A**) Phosphorylation of Akt^{S473} in gastrocnemii of *Ghsr*$^{-/-}$ mice injected with 100 μg/kg AG or UnAG or with saline. 60 minutes after treatment, gastrocnemii were removed and processed for Western blot analysis. Shown are representative blots and densitometric analysis of 3 independent experiments. (**B**–**D**) Mean percentage weight loss (**B**), CSA reduction (**C**), and CSA frequency distribution (**D**) of gastrocnemii from fed or 48-hour fasted *Ghsr*$^{-/-}$ mice injected s.c. twice daily with 100 μg/kg AG or UnAG or with saline (n = 5 per group). Frequency distribution was measured in 3 mice per group. In **B** and **C**, percent reduction is between fasted and fed mice. *P < 0.05, **P < 0.01 vs. saline treatment.

muscles of *Myh6/Ghrl* mice (data not shown). Indeed, we found that 2 distinct PI3K isoforms, namely PI3Kβ and PI3Kα, mediated the antiatrophic activity of AG/UnAG and IGF-1, respectively. This observation, along with the ability of a $G\alpha_s$-uncoupling drug to abolish the antiatrophic activity of AG/UnAG, but not IGF-1, is consistent with the hypothesis that the unknown receptor mediating the common activities of AG/UnAG is a GPCR (9). Moreover, these data further serve to rule out the hypothesis that AG/UnAG acts on myotubes by stimulating the autocrine release of IGF-1.

The inability of AG and UnAG to stimulate protein synthesis and hypertrophy in the skeletal muscle is consistent with their key role in the adaptive response to fasting and negative energy balance (13). The molecular mechanisms underlying the uncoupling of mTORC2 from mTORC1 remain to be investigated. AG and UnAG, which are released during fasting, might shift muscle metabolism toward amino acid oxidation, thereby decreasing the intracellular pool of free amino acids essential for mTORC1 activity (29). Alternatively, activation of PI3Kβ, whose enzymatic activity is lower than that of PI3Kα (54), may result in weaker activation of Akt. Finally, AMPK, which negatively regulates mTORC1 in skeletal muscle (55), may contribute to mTORC1 uncoupling, although AG was reported to be unable to stimulate AMPK in rat gastrocnemius (56).

The finding that p38 was required for AG/UnAG antiatrophic activity is consistent with previous findings that p38 cooperates with PI3K/Akt pathways to induce C2C12 differentiation (16, 57). However, the role of p38 in regulating muscle atrophy is complex, as its activation mediates muscle atrophy induced by oxidative stress and inflammatory cytokines (34, 36, 58). The role of p38 in signaling is determined by its association in distinct signaling complexes with different regulators and substrates and by its localization (35). Our findings are consistent with evidence indicating that, in myotubes, decreased p38 phosphorylation is associated with dexamethasone-induced atrophy, and that p38 mediates β-hydroxyl-β-methylbutyrate protection from dexamethasone-induced protein degradation (59, 60). Moreover, p38 activity can regulate cytoplasmic localization of FoxO3a independently of Akt, thereby impairing its transcriptional activity and Atrogin-1 induction (33, 61). Furthermore, activation of p38 stabilizes and activates the transcriptional coactivator PGC1α, which represses FoxO3a activity (62, 63). Although IGF-1 activated p38, this was dispensable for IGF-1 antiatrophic activity. In addition, IGF-1 and AG/UnAG antiatrophic activities differed in the inability of AG/UnAG to downregulate myostatin, a TGF-β–like inhibitor of muscle growth, which further supports the hypothesis that AG/UnAG and IGF-1 counteract muscle atrophy through distinct molecular mechanisms.

The data presented herein unveiled a novel component of the complex role of AG/UnAG, i.e., the direct activation of antiatrophic pathways in the skeletal muscle, eventually leading to reduced muscle wasting. This effect adds to the well-known capabilities of AG to stimulate appetite, regulate lipid metabolism, and release GH. Although the identity of the novel AG/UnAG receptor is yet unknown, these findings may have important biological and therapeutic implications, since they provide proof that UnAG has a strong and specific potential for the prevention or treatment of muscle atrophy, avoiding the diabetogenic side effects of AG (47) and the cancer risk associated with IGF-1 treatment (64).

Methods

Reagents. AG_{1-28} and $UnAG_{1-28}$ were purchased from PolyPeptide Laboratories. The PI3K p110α inhibitor PIK-75 hydrochloride was purchased from Axon Medchem, and the PI3K p110β inhibitor TGX-221 was a gift from U. Galli (Synthetic Medicinal Chemistry group, Università del Piemonte Orientale, Novara, Italy). Water-soluble dexamethasone and all other reagents, unless otherwise stated, were from Sigma-Aldrich. Anti–phospho-Akt^{S473}, anti-Akt, anti–phospho-FoxO3a^{T32}, anti-FoxO3a, anti–phospho-S6K^{T389}, anti-S6K, anti–phospho-S6$^{S235/236}$, anti-S6, anti-p38$^{T180/Y182}$, anti-p38, anti-raptor, and anti-rictor antibodies were from Cell Signaling Technology; anti-actin antibody was from Santa Cruz Biotechnology.

Cell cultures and myotube analysis. C2C12 myoblasts were differentiated in myotubes as previously described (16). For measurement of myotube diam-

eters, myotubes were fixed, and diameters were quantified by measuring a total of >100 myotube diameters from 5 random fields in 3 replicates at ×40 magnification using Image-Pro Plus software (MediaCybernetics) as described previously (24).

Raptor and rictor silencing. Raptor siRNA (*MISSION pre-designed siRNA* SASI_Mm01_00055293; Sigma-Aldrich), rictor siRNA (SASI_Mm01_00137731; Sigma-Aldrich), Block-iT, or siRNA negative control sequence (Invitrogen) were transfected with Lipofectamine2000 (Invitrogen) in C2C12 myotubes. Transfection efficiency was evaluated by the fluorescent siRNA negative control Block-iT, and silencing was verified by Western blot.

[^{3}H]-leucine incorporation assay. C2C12 myotubes were maintained for 24 hours with or without 10 nM AG or UnAG in differentiation medium supplemented with 2 μCi/ml [^{3}H]-leucine (Perkin Elmer) to evaluate the induction of protein synthesis. At the end of treatments, cells were washed with PBS, treated with 5% trichloroacetic acid, and lysed with 0.5 M NaOH and 0.5% SDS. The amount of incorporated [^{3}H]-leucine was evaluated by β counter (Tri-Carb 2800TR; Perkin Elmer) analysis. Data are the average of 4 replicates.

Western blot. C2C12 myotubes were serum starved overnight and then treated as indicated in the figure legends. Western blot was performed as previously described (16). Unless otherwise specified, after use of anti–phospho-specific antibodies, membranes were stripped with Re-Blot Plus (Chemicon, Millipore) and reblotted with the corresponding total protein antibodies.

Muscles of mice fasted for 6 hours were s.c. injected with 100 μg/kg UnAG or AG or with saline solution. At the indicated time points, gastrocnemii were removed, homogenized at 4°C in RIPA buffer (1% Triton X-100; 1% sodium deoxycholate; 0.1% SDS; 1 mM EDTA; 1 mM EGTA; 50 mM NaF; 160 mM NaCl; and 20 mM Tris-HCl, pH 7.4) containing 1 mM DTT, protease inhibitor cocktail, and 1 mM Na_3VO_4. Homogenates were then processed as above.

Tg animal generation and treatment. All experiments were conducted on young adult male FVB1 WT, FVB1 *Myh6/Ghrl*, and C57BL/6J *Ghsr*$^{-/-}$ mice (50), matched for age and weight.

Tg animals were obtained by cloning the murine ghrelin gene (*Ghrl*) under control of the cardiac promoter sequences of the β myosin heavy chain 3′ UTR and the first 3 exons of the α isoform *Myh6* (65). Transgene integration and expression were confirmed by PCR and real-time RT-PCR, respectively. Phenotypical characterization and experiments were carried out on hemizygote animals and littermate controls.

AG, UnAG, and IGF-1 plasmatic levels were measured by EIA kits (SPIbio Bertin Pharma for AG and UnAG; R&D Systems for IGF-1); insulin plasmatic levels were quantified with the Insulin (mouse) ELISA kit (ALPCO Diagnostics); and glycerol and free fatty acid plasmatic levels were evaluated by enzymatic assay kits (Cayman).

BMI was calculated as animal weight divided by the square of the nasoanal length.

Fasting-induced atrophy was achieved by 48 hours of food removal (63), while denervation-induced muscle atrophy was obtained by resection of the sciatic nerve under anesthesia with sevoflurane (Baxter) and evaluated 7 and 14 days later (66). Muscles were collected, weighed, and normalized for tibial length and processed either for RNA extraction or for histology.

Daily food intake was measured over a 12-day period, quantifying the food consumption of each mouse every day.

In all experiments with s.c. injection of AG and/or UnAG, controls were saline-injected animals.

Glucose and insulin tolerance tests. Glucose tolerance and insulin sensitivity tests were performed as previously described (43). For glucose tolerance evaluation, mice were injected i.p. with glucose at 1.5 mg/g body weight at 9:00 am, after 16 hours of fasting. Blood glucose was determined at the indicated time points on tail blood samples using the Accu-Chek Mobile blood glucose meter (Roche Diagnostics). For insulin sensitivity determination, Humulin R (0.75 U/kg body weight; Lilly) was administered i.p., and blood samples for glucose concentrations were collected as described above.

RNA extraction and analysis. Total RNA from cultured myotubes and from muscles was extracted by TRIreagent (Invitrogen). The RNA was retro-transcribed with High-Capacity cDNA Reverse Transcription Kit (Invitrogen), and real-time PCR was performed with the ABI7200 Sequence Detection System (Invitrogen) using the following assays: Mm00499518_m1 (*Fbxo32*, Atrogin-1), Mm01185221_m1 (*Trim63*, MuRF1), Mm00439560_m1 (*Igf1*), Mm00445450_m1 (*Ghrl*), Mm01254559_m1 (*Mstn*), Mm01247058_m1 (*Pck1*), Mm00446953_m1 (*Gusb*), and Mm00506384_m1 (*Ppif*).

Muscle sampling and staining for fiber size assessment. Muscles were embedded in Killik compound (Bio-optica) and frozen in liquid nitrogen–cooled isopentane. Serial transverse cryosections (7 μm thick) of the midbelly region of muscles were cut at –20°C and mounted on glass slides. The sections were air-dried, fixed for 10 minutes in 4% paraformaldehyde, and stained with H&E. The number of myofibers in TA, gastrocnemii, and EDL was measured from the histological preparations. Muscle fiber CSA was assessed as previously described (67). Data are expressed as fiber size distribution and as percent CSA reduction relative to controls.

Grip strength test. Skeletal muscle force was assessed using the BS-GRIP Grip Meter (2Biological Instruments) as previously described (68). Each animal was tested 3 times, and the average value of the maximum weight that the animal managed to hold was recorded and normalized to the mouse's weight.

Statistics. Data are presented as mean ± SEM. Variation among groups was evaluated using nonparametric Wilcoxon and Mann-Whitney *U* tests. Statistical significance was assumed for *P* values less than 0.05. All statistical analyses were performed with SPSS for Windows version 17.0.

Study approval. All animal experimental procedures were approved by the Institutional Animal Care and Use Committee at Università del Piemonte Orientale "Amedeo Avogadro."

Acknowledgments

We are grateful to Riccarda Granata and Cristina Grande for insulin measurements and to Thien-Thi Nguyen, Christian Zurlo, Laura Badà, and Giulia Bettas Ardisson for technical assistance. This work was supported by Telethon (grant no. GGP030386 to A. Graziani), Regione Piemonte CIPE (to A. Graziani, S. Geuna, and I. Perroteau), Regione Piemonte Ricerca Sanitaria (to A. Graziani), Italian Ministry for University and Research (PRIN grant to A. Graziani, S. Geuna, and I. Perroteau), and Opera Pia Eletto Lualdi.

Received for publication December 23, 2011, and accepted in revised form November 1, 2012.

Address correspondence to: Nicoletta Filigheddu, Department of Translational Medicine, Università del Piemonte Orientale "Amedeo Avogadro," Via Solaroli 17, 28100 Novara, Italy. Phone: 39.0321660529; Fax: 39.0321620421; E-mail: nicoletta.filigheddu@med.unipmn.it.

Paolo E. Porporato's present address is: Unit of Pharmacology and Therapeutics, Université Catholique de Louvain, Brussels, Belgium.

Viola F. Gnocchi's present address is: Research Center for Genetic Medicine, Children's National Medical Center, Washington, DC, USA.

Federica Chianale's present address is: Oncological Sciences Department, Systems Biology Unit, IRCC, Candiolo (TO), Italy.

1. Dodson S, et al. Muscle wasting in cancer cachexia: clinical implications, diagnosis, and emerging treatment strategies. *Annu Rev Med*. 2011;62:265–279.
2. Kojima M, Hosoda H, Date Y, Nakazato M. Ghrelin is a growth-hormone-releasing acylated peptide from stomach. *Nature*. 1999;402(6762):656–660.
3. Tschöp M, Smiley DL, Heiman ML. Ghrelin induces adiposity in rodents. *Nature*. 2000; 407(6806):908–913.
4. Nakazato M, Murakami N, Date Y, Kojima M. A role for ghrelin in the central regulation of feeding. *Nature*. 2001;409(6817):194–198.
5. Howard AD, Feighner SD, Cully DF, Arena JP. A receptor in pituitary and hypothalamus that functions in growth hormone release. *Science*. 1996; 273(5277):974–977.
6. Nagaya N, et al. Chronic administration of ghrelin improves left ventricular dysfunction and attenuates development of cardiac cachexia in rats with heart failure. *Circulation*. 2001;104(12):1430–1435.
7. Nagaya N, et al. Effects of ghrelin administration on left ventricular function, exercise capacity, and muscle wasting in patients with chronic heart failure. *Circulation*. 2004;110(24):3674–3679.
8. Baldanzi G, et al. Ghrelin and des-acyl ghrelin inhibit cell death in cardiomyocytes and endothelial cells through ERK1/2 and PI 3-kinase/AKT. *J Cell Biol*. 2002;159(6):1029–1037.
9. Granata R, et al. Acylated and unacylated ghrelin promote proliferation and inhibit apoptosis of pancreatic beta-cells and human islets: involvement of 3′,5′-cyclic adenosine monophosphate/protein kinase A, extracellular signal-regulated kinase 1/2, and phosphatidyl inositol 3-Kinase/Akt signaling. *Endocrinology*. 2007;148(2):512–529.
10. Chung H, Seo S, Moon M, Park S. Phosphatidylinositol-3-kinase/Akt/glycogen synthase kinase-3 beta and ERK1/2 pathways mediate protective effects of acylated and unacylated ghrelin against oxygen-glucose deprivation-induced apoptosis in primary rat cortical neuronal cells. *J Endocrinol*. 2008;198(3):511–521.
11. Yang J, Brown MS, Liang G, Grishin NV, Goldstein JL. Identification of the acyltransferase that octanoylates ghrelin, an appetite-stimulating peptide hormone. *Cell*. 2008;132(3):387–396.
12. Gutierrez JA, et al. Ghrelin octanoylation mediated by an orphan lipid transferase. *Proc Natl Acad Sci U S A*. 2008;105(17):6320–6325.
13. Chen C-Y, Asakawa A, Fujimiya M, Lee S-D, Inui A. Ghrelin gene products and the regulation of food intake and gut motility. *Pharmacol Rev*. 2009; 61(4):430–481.
14. Delhanty PJD, et al. Ghrelin and unacylated ghrelin stimulate human osteoblast growth via mitogen-activated protein kinase (MAPK)/phosphoinositide 3-kinase (PI3K) pathways in the absence of GHS-R1a. *J Endocrinol*. 2006;188(1):37–47.
15. Sato M, et al. Effects of ghrelin and des-acyl ghrelin on neurogenesis of the rat fetal spinal cord. *Biochem Biophys Res Commun*. 2006;350(3):598–603.
16. Filigheddu N, et al. Ghrelin and des-acyl ghrelin promote differentiation and fusion of C2C12 skeletal muscle cells. *Mol Biol Cell*. 2007;18(3):986–994.
17. Delhanty PJD, et al. Unacylated ghrelin rapidly modulates lipogenic and insulin signaling pathway gene expression in metabolically active tissues of GHSR deleted mice. *PLoS One*. 2010;5(7):e11749.
18. Nagaya N, et al. Treatment of cachexia with ghrelin in patients with COPD. *Chest*. 2005;128(3):1187–1193.
19. Balasubramaniam A, et al. Ghrelin inhibits skeletal muscle protein breakdown in rats with thermal injury through normalizing elevated expression of E3 ubiquitin ligases MuRF1 and MAFbx. *Am J Physiol Regul Integr Comp Physiol*. 2009;296(4):R893–R901.
20. Sugiyama M, et al. Ghrelin improves body weight loss and skeletal muscle catabolism associated with angiotensin II-induced cachexia in mice. *Regul Pept*. 2012;178(1–3):21–28.
21. DeBoer MD. Emergence of ghrelin as a treatment for cachexia syndromes. *Nutrition*. 2008;24(9):806–814.
22. Bodine SC, et al. Akt/mTOR pathway is a crucial regulator of skeletal muscle hypertrophy and can prevent muscle atrophy in vivo. *Nat Cell Biol*. 2001; t3(11):1014–1019.
23. Rommel C, et al. Mediation of IGF-1-induced skeletal myotube hypertrophy by PI(3)K/Akt/mTOR and PI(3)K/Akt/GSK3 pathways. *Nat Cell Biol*. 2001;3(11):1009–1013.
24. Sandri M, et al. Foxo transcription factors induce the atrophy-related ubiquitin ligase atrogin-1 and cause skeletal muscle atrophy. *Cell*. 2004;117(3):399–412.
25. Stitt TN, et al. The IGF-1/PI3K/Akt pathway prevents expression of muscle atrophy-induced ubiquitin ligases by inhibiting FOXO transcription factors. *Mol Cell*. 2004;14(3):395–403.
26. Latres E, et al. Insulin-like growth factor-1 (IGF-1) inversely regulates atrophy-induced genes via the phosphatidylinositol 3-kinase/Akt/mammalian target of rapamycin (PI3K/Akt/mTOR) pathway. *J Biol Chem*. 2005;280(4):2737–2744.
27. Bodine SC, et al. Identification of ubiquitin ligases required for skeletal muscle atrophy. *Science*. 2001;294(5547):1704–1708.
28. Foster KG, Fingar DC. Mammalian target of rapamycin (mTOR): conducting the cellular signaling symphony. *J Biol Chem*. 2010;285(19):14071–14077.
29. Laplante M, Sabatini DM. mTOR signaling in growth control and disease. *Cell*. 2012;149(2):274–293.
30. Copp J, Manning G, Hunter T. TORC-specific phosphorylation of mammalian target of rapamycin (mTOR): phospho-Ser2481 is a marker for intact mTOR signaling complex 2. *Cancer Res*. 2009; 69(5):1821–1827.
31. Sarbassov DD, et al. Prolonged rapamycin treatment inhibits mTORC2 assembly and Akt/PKB. *Mol Cell*. 2006;22(2):159–168.
32. Lamming DW, et al. Rapamycin-induced insulin resistance is mediated by mTORC2 loss and uncoupled from longevity. *Science*. 2012;335(6076):1638–1643.
33. Clavel S, Siffroi-Fernandez S, Coldefy AS, Boulukos K, Pisani DF, Dérijard B. Regulation of the intracellular localization of Foxo3a by stress-activated protein kinase signaling pathways in skeletal muscle cells. *Mol Cell Biol*. 2010;30(2):470–480.
34. Li YP, et al. TNF-alpha acts via p38 MAPK to stimulate expression of the ubiquitin ligase atrogin1/MAFbx in skeletal muscle. *FASEB J*. 2005; 19(3):362–370.
35. Cuadrado A, Nebreda AR. Mechanisms and functions of p38 MAPK signalling. *Biochem J*. 2010; 429(3):403–417.
36. McClung JM, Judge AR, Powers SK, Yan Z. p38 MAPK links oxidative stress to autophagy-related gene expression in cachectic muscle wasting. *Am J Physiol Cell Physiol*. 2010;298(3):C542–C549.
37. Kim J, et al. p38 MAPK participates in muscle-specific RING Finger 1-mediated atrophy in cast-immobilized rat gastrocnemius muscle. *Korean J Physiol Pharmacol*. 2009;13(6):491–496.
38. Hohenegger M, et al. 1998. Gsalpha-selective G protein antagonists. *Proc Natl Acad Sci U S A*. 1998; 95(1):346–351.
39. Jia S, et al. Essential roles of PI(3)K-p110beta in cell growth, metabolism and tumorigenesis. *Nature*. 2008;454(7205):776–779.
40. Ciraolo E, et al. Phosphoinositide 3-kinase p110beta activity: key role in metabolism and mammary gland cancer but not development. *Sci Signal*. 2008;1(36):ra3.
41. Morissette MR, Cook SA, Buranasombati C, Rosenberg MA, Rosenzweig A. Myostatin inhibits IGF-I-induced myotube hypertrophy through Akt. *Am J Physiol Cell Physiol*. 2009;297(5):1124–1132.
42. Trendelenburg AU, Meyer A, Rohner D, Boyle J, Hatakeyama S, Glass DJ. Myostatin reduces Akt/TORC1/p70S6K signaling, inhibiting myoblast differentiation and myotube size. *Am J Physiol Cell Physiol*. 2009;296(6):C1258–C1270.
43. Zhang W, Chai B, Li J-Y, Wang H, Mulholland MW. Effect of des-acyl ghrelin on adiposity and glucose metabolism. *Endocrinology*. 2008;149(9):4710–4716.
44. Iwakura H, et al. Analysis of rat insulin II promoter-ghrelin transgenic mice and rat glucagon promoter-ghrelin transgenic mice. *J Biol Chem*. 2005; 280(15):15247–15256.
45. Ariyasu H, et al. Transgenic mice overexpressing des-acyl ghrelin show small phenotype. *Endocrinology*. 2005;146(1):355–364.
46. Musarò A, et al. Localized Igf-1 transgene expression sustains hypertrophy and regeneration in senescent skeletal muscle. *Nat Genet*. 2001;27(2):195–200.
47. Delhanty PJ, van der Lely AJ. Ghrelin and glucose homeostasis. *Peptides*. 2011;32(11):2309–2318.
48. Mandard S, et al. The fasting-induced adipose factor/angiopoietin-like protein 4 is physically associated with lipoproteins and governs plasma lipid levels and adiposity. *J Biol Chem*. 2006;281(2):934–944.
49. Sharara-Chami RI, Zhou Y, Ebert S, Pacak K, Ozcan U, Majzoub JA. Epinephrine deficiency results in intact glucose counter-regulation, severe hepatic steatosis and possible defective autophagy in fasting mice. *Int J Biochem Cell Biol*. 2012;44(6):905–913.
50. Sun Y, Wang P, Zheng H, Smith RG. Ghrelin stimulation of growth hormone release and appetite is mediated through the growth hormone secretagogue receptor. *Proc Natl Acad Sci U S A*. 2004; 101(13):4679–4684.
51. Sheriff S, Kadeer N, Joshi R, Friend LA, James JH, Balasubramaniam A. Des-acyl ghrelin exhibits pro-anabolic and anti-catabolic effects on C2C12 myotubes exposed to cytokines and reduces burn-induced muscle proteolysis in rats. *Mol Cell Endocrinol*. 2012;351(2):286–295.
52. Pallafacchina G, Calabria E, Serrano AL, Kalhovde JM, Schiaffino S. A protein kinase B-dependent and rapamycin-sensitive pathway controls skeletal muscle growth but not fiber type specification. *Proc Natl Acad Sci U S A*. 2002;99(14):9213–9218.
53. Skurk C, et al. The FOXO3a transcription factor regulates cardiac myocyte size downstream of AKT signaling. *J Biol Chem*. 2005;280(21):20814–20823.
54. Zhao JJ, et al. The p110alpha isoform of PI3K is essential for proper growth factor signaling and oncogenic transformation. *Proc Natl Acad Sci U S A*. 2006;103(44):16296–16300.
55. Gwinn DM, et al. AMPK phosphorylation of raptor mediates a metabolic checkpoint. *Mol Cell*. 2008; 30(2):214–226.
56. Barazzoni R, et al. Ghrelin regulates mitochondrial-lipid metabolism gene expression and tissue fat distribution in liver and skeletal muscle. *Am J Physiol Endocrinol Metab*. 2005;288(1):E228–E235.
57. Serra C, et al. Functional interdependence at the chromatin level between the MKK6/p38 and IGF1/PI3K/AKT pathways during muscle differentiation. *Mol Cell*. 2007;28(2):200–213.
58. Puigserver P, et al. Cytokine stimulation of energy expenditure through p38 MAP kinase activation of PPARgamma coactivator-1. *Mol Cell*. 2001; 8(5):971–982.
59. Kewalramani G, et al. Acute dexamethasone-induced increase in cardiac lipoprotein lipase requires activation of both Akt and stress kinases. *Am J Physiol Endocrinol Metab*. 2008;295(1):E137–E147.
60. Aversa Z, Alamdari N, Castillero E, Muscaritoli M, Rossi Fanelli F, Hasselgren PO. beta-Hydroxy-beta-methylbutyrate (HMB) prevents dexamethasone-induced myotube atrophy. *Biochem Biophys Res Commun*. 2012;423(4):739–743.
61. Qin W, Pan J, Wu Y, Bauman WA, Cardozo C. Protection against dexamethasone-induced muscle atrophy is related to modulation by testosterone of FOXO1 and PGC-1α. *Biochem Biophys Res Commun*.

2010;403(3–4):473–478.
62. Hong T, et al. Fine-tuned regulation of the PGC-1α gene transcription by different intracellular signaling pathways. *Am J Physiol Endocrinol Metab*. 2011;300(3):E500–E507.
63. Sandri M, et al. PGC-1alpha protects skeletal muscle from atrophy by suppressing FoxO3 action and atrophy-specific gene transcription. *Proc Natl Acad Sci U S A*. 2006;103(44):16260–16265.
64. Fürstenberger G, Senn HJ. Insulin-like growth factors and cancer. *Lancet Oncol*. 2002;3(5):298–302.
65. De Acetis M, et al. Cardiac overexpression of melusin protects from dilated cardiomyopathy due to long-standing pressure overload. *Circ Res*. 2005; 96(10):1087–1094.
66. Hishiya A, Iemura S, Natsume T, Takayama S, Ikeda K, Watanabe K. A novel ubiquitin-binding protein ZNF216 functioning in muscle atrophy. *EMBO J*. 2006;25(3):554–564.
67. Geuna S, Tos P, Guglielmone R, Battiston B, Giacobini-Robecchi MG. Methodological issues in size estimation of myelinated nerve fibers in peripheral nerves. *Anat Embryol (Berl)*. 2001;204(1):1–10.
68. Tos P, et al. Employment of the mouse median nerve model for the experimental assessment of peripheral nerve regeneration. *J Neurosci Methods*. 2008;169(1):119–127.